Electrocatalytic Oxygen Evolution Reaction (OER) on Mixed Nanoporous RuIr Borides

Saad Intikhab¹, Maxim Sokol², Varun Natu², Swarnendu Chatterjee¹, Yawei Li¹, Michel W.

Barsoum², Joshua Snyder^{1*}

¹ Department of Chemical and Biological Engineering, Drexel University, Philadelphia, PA,

19104, USA

² Department of Materials Science and Engineering, Drexel University, Philadelphia, PA, 19104,

USA

Corresponding Author email: jds43@drexel.edu

Abstract

Efficient water splitting for commercial electrolysis devices is predicated on the

development of materials, specifically for the catalytic electrodes, that exhibit an optimal balance

between activity and stability. Complicating the development of electrocatalytic materials,

particularly for oxygen evolving anodes in acidic polymer electrolyte membrane eletrolyzers, is

an inverse relationship between activity and stability. Here the development of a nanostructured

oxygen evolution reaction (OER) electrocatalyst for low pH water splitting is demonstrated.

Dealloying of mixed RuIr borides is used to form a high aspect ratio electrocatalytic material that

exhibits low OER overpotentials matching that for RuO_x and electrolytic stability matching that

of IrO_x.

Keywords: Oxygen evolution reaction; dealloying; nanoporous metals; PEM electrolysis

1. Introduction

Proton exchange membrane (PEM) electrolyzers have the potential to play a key role in

both the storage of intermittent renewables like solar and wind^{1,2} and the production of fuel for

small to large scale transportation^{3–7}. However, the development and widescale commercialization

of PEM electrolyzers is limited by the sluggish kinetics of the anodic oxygen evolution reaction

1

(OER)^{8–10}. To improve the efficacy of OER in electrolyzers, it is important to develop materials which show high catalytic activity while maintaining a suitable operational longevity. However, it is observed that the most active catalysts are not necessarily the most stable and a general inverse relationship between OER electrocatalyst activity and stability is well documented^{8,9,11,12}. Therefore, any path forward must focus on identifying the optimal balance between electrolyzer anode catalyst activity and durability.

Previous work has identified oxygenated intermediate binding energy as a key OER activity descriptor, with DFT analysis providing convincing correlations^{11,13}. Both RuO_x and IrO_x have electronic properties such that they bind oxygenated intermediates neither too strongly nor too weakly^{14,15}. They are widely regarded as benchmark OER electrocatalysts^{8–12,15–17}. While RuO_x is more active than IrO_x, it is less stable and dissolves more readily in acidic electrolytes⁹. To improve the stability of RuO_x, while maintaining much of the intrinsic activity, alloys and mixed oxides, Ru_xIr_{1-x}O₂, have been found to effectively suppress high rates of corrosion without significantly impacting OER performance^{8,15–19}. For example, Danilovic et al. have shown that for the Ru-Ir alloy system, potential cycling leads to the formation of an 'Ir-protective skeleton' which quadruples the stability compared to commercial Ru-Ir alloy anode catalysts⁸. The thin Ir-skeleton surface and the presence of the subsurface Ru maintain the impact of Ru on OER activity through electronic interaction between the Ru and Ir while the more stable surface Ir protects the underlying Ru. This strategy has proved generally effective in approaching the balance between OER electrocatalyst activity and durability.

Among the synthesis methods proposed for the development of catalyst materials for OER, electrochemical dealloying of multimetallic alloys to evolve various nanoporous architectures with Ir-based oxides is particularly promising ^{12,20,21}. Selective etching, or dealloying, involves the

dissolution of a less noble component and simultaneous surface diffusion and island formation of the remaining more noble component from the parent alloy leading to the formation of 3-dimensional (3-D) nanoporous structures^{22–25}. Dealloying has demonstrated utility in the synthesis of complex morphology nanoporous electrocatalytic materials. Nanoporous metals with oxidized surfaces possess high intrinsic surface-to-volume ratios, yielding enhanced mass-normalized activity. Additionally, the metallic backbone of the nanoporous architecture limits high current density losses associated with the high resistivity of other transition metal oxide-based electrocatalysts^{26–30}. Surface limited dealloying has also been used to create defected surfaces that exhibit enhanced activity due to the reduction in the average surface coordination number^{8,29}.

In this study, we synthesize Ru- and Ir- based nanoporous OER electrocatalysts with controlled RuIr composition through the electrochemical dealloying of ternary boride, Ru_xIr_{1-x}B, precursors. Our results suggest that the bimetallic boride (Ru_{0.6}Ir_{0.4}B) allows the integration of the corresponding advantages of both IrO_x and RuO_x, yielding a superior balance between activity and durability. The synthesized catalyst shows excellent OER performance and a prolonged catalyst life at OER operational conditions compared to their monometallic counterparts.

2. Experimental Methods

2.1 Synthesis of Ir-Ru borides

For the synthesis of the ruthenium boride (RuB), powders of Ru (99.9%, metal basis, Alfa Aesar, -325 mesh) and B (>98 %, crystalline, Alfa Aesar, -400 mesh) are mixed in a 1:1.03 molar ratio for 24 h in a plastic jar with yttria-stabilized zirconia balls (balls to powders ratio of 10:1). The mixed powders are cold pressed in a cylindrical steel die to 400 MPa, loaded into a high purity alumina boat, and heated at a rate of 5 °C s⁻¹, in an alumina tube furnace under flowing Ar to 1673

K with a holding time of 5 h. Upon cooling, the reacted pellet is ground into powders using a carbide endmill and sieved through a No. 230 mesh.

The iridium boride (IrB) is synthesized from a mixture of Ir (99.9%, metal basis, Alfa Aesar, -325 mesh) and B (>98 %, crystalline, Alfa Aesar, -400 mesh) in a 1:0.9 molar ratio. The synthesis steps are similar to RuB, except in this case the reaction temperature is 1773 K. The pellet is then ground into powders using a carbide endmill and sieved through a No. 230 mesh.

For the synthesis of Ru_{0.6}Ir_{0.4}B, sieved RuB and IrB powders are mixed in a 3:2 molar ratio. The mixed powders are cold pressed at 400 MPa and heated under flowing Ar to 1773 K with a holding time of 5 h in an alumina tube furnace. Upon cooling, the reacted pellet is ground into powders using a carbide endmill and sieved through a No. 230 mesh.

2.2 Electrochemical measurements

The electrochemical measurements are performed in a three-electrode FEP (fluorinated ethylene propylene copolymer) cell with an Autolab (PGSTAT302N) potentiostat using a rotating disc electrode (RDE) setup. Catalytic inks are prepared by diluting the boride powders in isopropanol, 1 mg mL⁻¹. 5 µl of Nafion solution (5 wt.% in isopropanol) is added for every 1 ml of ink. A known volume of ink is drop-cast onto a glassy carbon (GC) disc (5 mm diameter) to obtain a loading of 1 mg cm⁻² and dried under Ar (Research grade, Airgas) flow. The GC disk is then mounted in a hanging meniscus holder and transferred into the FEP cell containing a Ar purged electrolyte under potential control.

The electrolytes are prepared with high purity HClO₄ (70 wt%, Suprapur, Merck) and 18.2 MΩ cm Milli-Q water. Carbon paper is used as the counter electrode and a Ag/AgCl reference (BASi) electrode is used for all measurements. All potentials, reported in the manuscript, have been converted to the reversible hydrogen electrode (RHE) scale. All voltages are corrected for iR

drop. The OER polarization curves are measured through linear sweep voltammetry from 0.5 V to an upper potential limit (where the current density of 10 mA cm⁻² is obtained) at a scan rate of 20 mV s⁻¹ in Ar purged electrolyte at a rotation rate of 1600 rpm.

2.3 Materials Characterization

Phase compositions are determined by X-ray diffraction (XRD) pattern acquired using a powder diffractometer (Rigaku SmartLab, Tokyo, Japan) in the Bragg–Brentano geometry with Cu Kα radiations in the 10–70° 2θ range using a 0.02° step size and a dwell time of 7.5 s per step. A transmission electron microscope (TEM) (JEOL JEM2100) is used to characterize the morphology of the as-synthesized and dealloyed borides. A Physical Electronics VersaProbe 5000 (Physical Electronics, Chanhassen, Minnesota, USA) instrument is used to obtain high-resolution XPS spectra. All the samples are analyzed after sputtering with a 1 kV Ar⁺ ion beam for 60 s. Monochromatic Al-Kα X-rays with the spot size of 200 μm are used to irradiate the sample surface. Pass energy of 23.5 eV, with a step size of 0.5 eV is used to gather the high-resolution spectra. CasaXPS Version 2.3.19PR1.0 software is used for peak fitting. The XPS spectra are calibrated by setting the valence edge to zero, which is calculated by fitting the valence edge with a step down function and setting the intersection to 0 eV³⁰.

Results and Discussion

Experimental and theoretical XRD patterns of the various boride phases studied herein are presented in **Figure 1**. All synthesized materials are essentially phase pure with only RuB exhibiting around 1 wt.% of Ru₁₁B₈ (Rietveld). The mixed Ru_{0.6}Ir_{0.4}B is found to be a solid solution with the same hexagonal structure (P-6m2 space group) as RuB and no detectable phase impurities. Slight variations of peak positions in the Ru_{0.6}Ir_{0.4}B XRD pattern, as well as peak broadening are observed. These variations can be attributed to atom size effects which modify the lattice

parameters, whereas the intensity changes reflect the respective influence of Ir replacing Ru onto the structure factor. The composition of the Ru_{0.6}Ir_{0.4}B is chosen as it exhibits solid solution homogeneity following our synthesis protocol, is slightly Ru-rich to yield a dominant impact of Ru on OER activity, and also possess a composition within the parting limit for nanoporosity evolution^{33,34}.

The OER activity of the as-synthesized borides (RuB, Ru_{0.6}Ir_{0.4}B, IrB), as measured in the RDE half-cell in 0.1 M HClO₄, are shown in Figure 2(a). The presented polarization curves are identical in Ar purged or O₂ saturated electrolyte. For the as-synthesized borides, the observed trend in OER activity scales with the Ru content, decreasing the onset potential from 1.43 V for IrB to 1.3 V for RuB. The measured overpotentials, at 10 mA cm⁻², are 210, 280, and 390 mV for RuB, Ru_{0.6}Ir_{0.4}B, and IrB, respectively. These results are consistent with what has been observed by others for Ru and Ir-based oxide catalysts¹⁸. This is an indication that either: (1) Boron is not having any electronic or strain impact on the activity of the neighboring Ru or Ir, or (2) quick potential-driven removal of boron from the surface and near surface of the catalyst minimizes any of its potential impact. Following the initial OER polarization curves, each boride-based catalyst is subjected to a load cycling protocol (Ar saturated 0.1 M HClO₄, 800 rpm, 100 mV s⁻¹, 0.5 to 1.5 V vs RHE, 1000 cycles). During load cycling, an increase in the capacitive charging current is observed, Figure S1. Post-cycling TEM analysis of the RuB and Ru_{0.6}Ir_{0.4}B, Figure 3, shows that the increase in capacitive current is due to the evolution of nanoporosity, resulting in an increase in materials' active area. The dealloyed material is henceforth denoted as d-RuB, d-RuIrB, and d-IrB. As shown in Figure 2(b), after 1000 load cycles, the geometric area normalized OER current density increases. This is likely the result of the increased active area due to the nanoporosity evolution in the RuB and Ru_{0.6}Ir_{0.4}B precursor materials. The cycling protocol (0.5 V to 1.65 V) is

also applied to IrB with a higher upper potential limit owing to the higher onset potential for OER. Repeated cycling, however, does not evolve porosity in IrB as indicated by the absence of an increase in the capacitive current, Figure S1. For the IrB, OER activity is found to decrease following the load cycling profile. This is likely a consequence of the passivation of the surface in an IrO_x phase following the gradual smoothening of the atomic surface roughness that evolves through removal of near surface B, where this atomic roughness is known to support higher activities⁸, through an electrochemical annealing process^{33,34}. Dealloying and nanoporosity evolution in Ir-based alloys is notoriously difficult¹². This is due to the low surface diffusivity of Ir, which tends to result in a cessation in the dealloying/nanoporosity evolution at early stages as the surface of the alloyed material becomes passivated by the slow diffusing Ir^{12, 27,31}. Surface diffusivity roughly scales with melting point^{27,31}. Etch front propagation into an alloy during dealloying requires dissolution of a sacrificial component and fast surface diffusion-driven rearrangement of the remaining component(s) to continue to expose the underlying alloy. Additionally, the formation of a surface oxide on Ir can act to further limit diffusive surface rearrangement. In contrast, for Ru, the susceptibility of Ru to dissolve, at least to a limited extent, during dealloying will help to propagate the etch front into the material and, in turn, allow the nanoporosity to evolve.

The "aging" during load cycling can be further probed with XPS, both pre- and post-load cycling (viz. after 2 and 1000 cycles). **Figures S2, S3, and S4** show the Ru, Ir, and Ru/Ir spectra for RuB, IrB, and Ru_{0.6}Ir_{0.4}B, respectively. **Table S1-3** summarizes the XPS peak fitting results. A general decrease in the proportion of Ru-B and Ir-B components, and an increase in their corresponding oxide contributions, is observed with potential cycling. For the RuB electrode, only two OER cycles are enough to oxidize Ru and reduce the Ru-B peak by 50%. After 1000 cycles,

the peak associated with Ru-B vanishes indicating that the majority of the B in the sample has been etched away. For RuB, loss of B is associated with the evolution of nanoporosity, where B is the dealloyed component and the remaining Ru evolves to form a nanoporous architecture, Figure 3(d). For the IrB electrode, due to the higher Ir mobility, the degree of oxidation is significantly lower and there is only a moderate decrease in the peak associated with Ir-B, ~2% after 2 cycles and ~7% after 1000 cycles. In agreement with the post-cycling TEM micrographs shown in **Figure** 3(f), the surface passivation by the more noble and slow moving Ir prevents movement of the etch front into the material, protecting and preserving the majority of the B from the precursor material. The presence of Ir in Ru_{0.6}Ir_{0.4}B reduces the degree of Ru oxidation while also reducing the total loss of B during load cycling in comparison to the RuB precursor. This behavior is characteristic of traditional dealloying systems^{33,34,38,39} where here B acts as the sacrificial component leading to the formation of nanoporosity. Dealloying intrinsically leads to the formation of core-shell structures due to the layer-by-layer etching/porosity evolution mechanism³², as evidenced by the higher residual B content in the Ru_{0.6}Ir_{0.4}B following load cycling. The upper potential limit used here in the load cycling protocol is well above the potentials required to oxidize any exposed Ru or Ir on the surface of the porous material³², as confirmed by the XPS analysis. To summarize, the potential cycling protocol on Ru_{0.6}Ir_{0.4}B results in a IrO_x-RuO_x shell and a Ru_xIr_{1-x}B core. The formation of IrO_x on the surface of the dealloyed structure likely slows the dissolution of Ru and B from the core. Nonetheless, after 1000 cycles, XPS spectra for Ru and Ir for Ru_{0.6}Ir_{0.4}B shows a degree of oxidation of Ru of ~93% with that for Ir being ~30%.

The electrochemically induced removal of B from the Ru- and RuIr-borides through load cycling leads to the evolution of a nanoporous structure in a process analogous to traditional dealloying in binary alloys^{24, 34,35,37}. It has been shown previously, that the nanoporous

architecture, composed of an open bi-continuous structure and a continuous metallic backbone, can at least partially alleviate OER performance losses that are associated with the high resistivity of agglomerated transition metal oxide electrocatalysts¹². The potential for enhanced in-plane and through-plane conductivity in addition to the increased surface area-to-mass ratio render these boride-derived nanoporous catalysts attractive for polymer electrolyte membrane (PEM) electrolysis. Viability in a PEM electrolyzer requires that the OER electrocatalysts exhibit a minimal loss in operational current density during long-term, constant potential electrolysis. The operational durability of the boride-derived catalysts is analyzed during constant potential electrolysis, **Figure 4**. The materials tested are those following the 1000 cycle dealloying/load cycling protocol. For d-RuB, the current density quickly begins to decay at 1.5 V, decreasing close to zero after ~2 h. This is in line with previous studies where it has been shown that at potentials > 1.45 V, the valence oxidation state of Ru changes to the unstable $n > 4^+$ from $n = 4^+$, which triggers the dissolution of Ru⁴. For d-IrB, the current starts to decay initially, but then stabilizes after 15 mins. A higher potential (1.6 V) is applied for d-IrB since the OER onset potential of d-IrB is much higher than that for the d-Ru-borides. Although there is dissolution of Ir as well, the rate of Ir dissolution^{9,11} is slow enough that the d-IrB shows acceptable stability at constant potential. In Figure 4, it is also apparent that d-RuIrB has a similar degree of durability at 1.5 V, while maintaining a much higher current density. The jump in currents observed for d-RuIrB in Figure 4 are due to transient bubble formation and detachment. Taken together, the durability of the d-RuIrB, Figure 4, is similar to that of d-IrB while the activity of d-RuIrB, Figure 2, matches that of both RuB and d-RuB. This highlights the viability of our strategy, where the combination of Ru and Ir into a nanoporous architecture strikes a unique balance of activity and durability that is difficult to match with single component catalysts. Unique to the approach presented here is the

ease with which multiple components can be integrated into the precursor material which can then be electrochemically evolved into a high surface area, active OER electrocatalyst. Future work will focus on additional metallic additives to further push the boundaries of activity/stability balance optimization.

Conclusion

This study reports the development of nanoporous OER catalysts through the dealloying of metallic boride precursor materials. It is found that the derived nanoporous architecture obtained through the electrochemical dealloying of Ru_{0.6}Ir_{0.4}B, forming d-RuIrB, shows a remarkable balance between OER activity and prolonged durability, nearly matching the activity of d-RuB and the stability of d-IrB. This result is likely due to the synergistic effect of both Ru and Ir in the bimetallic boride. Key to the utility of this strategy is the ease with which multi-component catalysts can be formed by the simple incorporation of species into the boride precursors and the subsequent dealloying to form the high surface area OER electrocatalysts. The approach presented here may be applied as a general strategy towards tuning activity and durability of multi-metallic nanoporous electrocatalysts.

Acknowledgements

J.S., S.I., S.C., and Y.L. acknowledge support from the National Science Foundation, Division of Materials Research under the award number 1904571.

References

- 1. Intikhab, S., Natu, V., Li, J., Li, Y., Tao, Q., Rosen, J., Barsoum, M., Snyder, J. Stoichiometry and surface structure dependence of hydrogen evolution reaction activity and stability of Mo x C MXenes. *J. Catal.* **371,** 325–332 (2019).
- Li, Y., Polakovic, T., Curtis, J., Shumlas, S., Chatterjee, S., Intikhab, S., Chareev, D.,
 Volkova, O., Vasiliev, A., Karapetrov, K., Snyder, J. Tuning the activity/stability balance
 of anion doped CoSxSe2-xdichalcogenides. *J. Catal.* 366, 50–60 (2018).
- 3. Sharma, S., Ghoshal, S. Hydrogen the future transportation fuel: from production to applications. *Renew. Sustain. Energy Rev.* **43**, 1151–1158 (15AD).
- 4. Abdalla, A., Hossain, S., Nisfindy, O., Azad, A., Dawood, M., Azad, A. Hydrogen production, storage, transportation and key challenges with applications: a review. *Energy Convers. Manag.* **165**, 602–627 (2018).
- 5. Li, X., Allen, J., Stager, J., Ku, A. Paths to low-cost hydrogen energy at a scale for transportation applications in the USA and China via liquid-hydrogen distribution networks. *Clean Energy* **4**, 26–47 (2020).
- 6. Sinigaglia, T., Lewiski, F., Martins, M., Siluk, J. Production, storage, fuel stations of hydrogen and its utilization in automotive applications a review. *Int. J. Hydrog. Energy* **42,** 24597–24611 (2017).
- 7. Pivovar, B., Rustagi, N., Satyapal, S. Hydrogen at Scale (H2@scale): Key to a clean, economic, and sustainable energy system. *Electrochem. Soc. Interface* **27**, 47–53 (2018).
- 8. Danilovic, N., Subbaraman, R., Chang, K. C., Chang, S. H., Kang, Y., Snyder, J., Paulikas, A. P., Strmcnik, D., Kim, Y. T., Myers, D., Stamenkovic, V. R. & Markovic, N. M. Using surface segregation to design stable Ru-Ir oxides for the oxygen evolution

- reaction in acidic environments. Angew. Chemie Int. Ed. 53, 14016–14021 (2014).
- Danilovic, Nemanja, Subbaraman, Ramachandran, Chang, Kee Chul, Chang, Seo Hyoung, Kang, Yijin J., Snyder, Joshua, Paulikas, Arvydas P., Strmcnik, Dusan, Kim, Yong Tae, Myers, Deborah, Stamenkovic, Vojislav R., Markovic, N. M. Activity-stability trends for the oxygen evolution reaction on monometallic oxides in acidic environments. *J. Phys.* Chem. Lett. 5, 2474–2478 (2014).
- Frydendal, R., Paoli, E. A., Knudsen, B. P., Wickman, B., Malacrida, P., Stephens, I. E. L.
 & Chorkendorff, I. Benchmarking the Stability of Oxygen Evolution Reaction Catalysts:
 The Importance of Monitoring Mass Losses. *ChemElectroChem* 1, 2075–2081 (2014).
- 11. Reier, T., Oezaslan, M. & Strasser, P. Electrocatalytic oxygen evolution reaction (OER) on Ru, Ir, and pt catalysts: A comparative study of nanoparticles and bulk materials. *ACS Catal.* **2,** 1765–1772 (2012).
- 12. Kim, Y. T., Lopes, P. P., Park, S. A., Lee, A. Y., Lim, J., Lee, H., Back, S., Jung, Y., Danilovic, N., Stamenkovic, V., Erlebacher, J., Snyder, J. & Markovic, N. M. Balancing activity, stability and conductivity of nanoporous core-shell iridium/iridium oxide oxygen evolution catalysts. *Nat. Commun.* **8**, 1449 (2017).
- 13. Rossmeisl, J., Qu, Z. W., Zhu, H., Kroes, G. J. & Nørskov, J. K. Electrolysis of water on oxide surfaces. *J. Electroanal. Chem.* **607**, 83–89 (2007).
- 14. Rogers, D. B., Shannon, R. D., Sleight, A. W. & Gillson, J. L. Crystal chemistry of metal dioxides with rutile-related structures. *Inorg. Chem.* **8**, 841–849 (1969).
- Audichon, T., Napporn, T. W., Canaff, C., Morais, C., Comminges, C. & Kokoh, K. B.
 IrO2 Coated on RuO2 as Efficient and Stable Electroactive Nanocatalysts for
 Electrochemical Water Splitting. J. Phys. Chem. C 120, 2562–2573 (2016).

- 16. Li, G., Li, S., Ge, J., Liu, C. & Xing, W. Discontinuously covered IrO2-RuO2@Ru electrocatalysts for the oxygen evolution reaction: How high activity and long-term durability can be simultaneously realized in the synergistic and hybrid nano-structure. *J. Mater. Chem. A* 5, 17221–17229 (2017).
- 17. Owe, L., Tsypkin, M., Wallwork, K., Haverkamp, R., Sunde, S. Iridium-ruthenium single phase mixed oxides for oxygen evolution: composition dependence of electrocatalytic activity. *Electrochim. Acta* **70**, 158–164 (2012).
- 18. Suen, N.-T., Hung, S.-F., Quan, Q., Zhang, N., Xu, Y.-J. & Chen, H. M. Electrocatalysis for the oxygen evolution reaction: recent development and future perspectives. *Chem. Soc. Rev.* **46**, 337–365 (2017).
- 19. Mayousse, E., Maillard, F., Fouda-Onana, F., Sicardy, O., Buillet, N. Synthesis and characterization of electrocatalysts for the oxygen evolution in PEM water electrolysis. *Int. J. Hydrog. Energy* **36**, 10474–10481 (2011).
- Spöri, C., Kwan, J. T. H., Bonakdarpour, A., Wilkinson, D. P. & Strasser, P. The Stability Challenges of Oxygen Evolving Catalysts: Towards a Common Fundamental Understanding and Mitigation of Catalyst Degradation. *Angew. Chemie - Int. Ed.* 56, 5994–6021 (2017).
- Feng, J., Lv, F., Zhang, W., Li, P., Wang, K., Yang, C., Wang, B., Yang, Y., Zhou, J., Lin,
 F., Wang, G.-C. & Guo, S. Iridium-Based Multimetallic Porous Hollow Nanocrystals for
 Efficient Overall-Water-Splitting Catalysis. Adv. Mater. 29, 1703798 (2017).
- 22. Snyder, J., Fujita, T., Chen, M. W. & Erlebacher, J. Oxygen reduction in nanoporous metal-ionic liquid composite electrocatalysts. *Nat. Mater.* **9**, (2010).
- 23. Erlebacher, J., Aziz, M., Karma, A., Dimitrov, N., Sieradzki, K. Evolution of nanoporosity

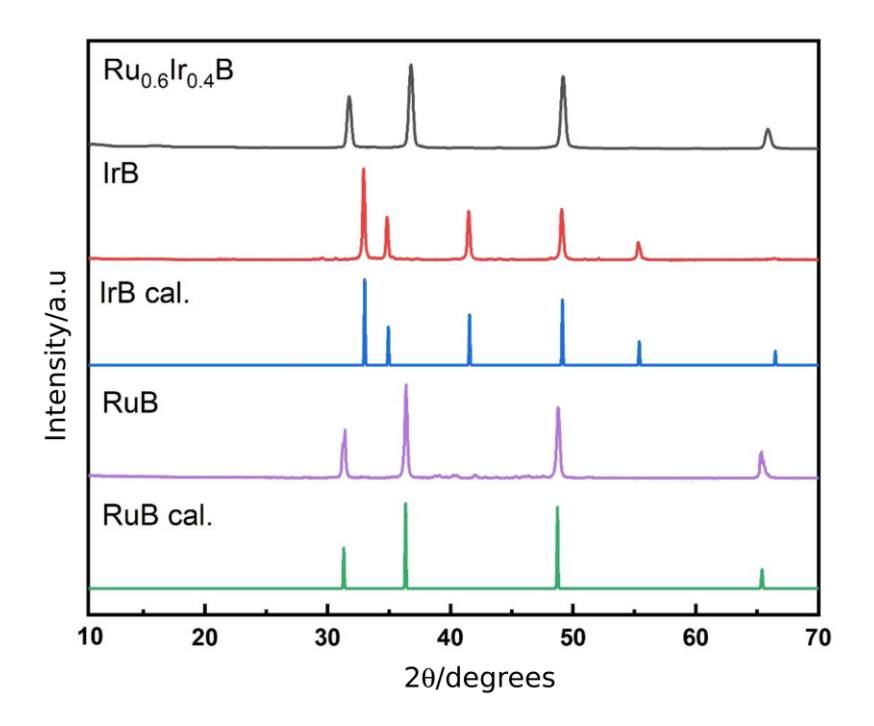
- in dealloying. *Nature* **410**, 450–453 (2001).
- 24. Snyder, J., Livi, K., Erlebacher, J. Dealloying Silver/Gold Alloys in Neutral Silver Nitrate Solution: Porosity Evolution, Surface Composition, and Surface Oxides. *J. Electrochem.*Soc. 155, C464–C473 (2008).
- 25. Chatterjee, S., Griego, C., Hart, J. L., Li, Y., Taheri, M. L., Keith, J. & Snyder, J. D. Free Standing Nanoporous Palladium Alloys as CO Poisoning Tolerant Electrocatalysts for the Electrochemical Reduction of CO2 to Formate. *ACS Catal.* **9,** 5290–5301 (2019).
- 26. Snyder, J., McCue, I., Livi, K. & Erlebacher, J. Structure/Processing/Properties Relationships in Nanoporous Nanoparticles As Applied to Catalysis of the Cathodic Oxygen Reduction Reaction. J. Am. Chem. Soc. 134, 8633–8645 (2012).
- 27. Chatterjee, S., Anikin, A., Ghoshal, D., Hart, J. L., Li, Y., Intikhab, S., Chareev, D. A., Volkova, O. S., Vasiliev, A. N., Taheri, M. L., Koratkar, N., Karapetrov, G. & Snyder, J. Nanoporous metals from thermal decomposition of transition metal dichalcogenides. *Acta Mater.* 184, 79–85 (2020).
- Kang, Y., Snyder, J., Chi, M., Li, D., More, K., Markovic, N., Stamenkovic, V.
 Multimetallic core/interlayer/shell nanostructures as advanced electrocatalysts. *Nano Lett.* 14, 6361–6367 (2014).
- 29. Kim, Y.-T., Lopes, P. P., Park, S.-A., Lee, A.-Y., Lim, J., Lee, H., Back, S., Jung, Y., Danilovic, N., Stamenkovic, V., Erlebacher, J., Snyder, J. & Markovic, N. M. Balancing activity, stability and conductivity of nanoporous core-shell iridium/iridium oxide oxygen evolution catalysts. *Nat. Commun.* **8**, 1449 (2017).
- Chatterjee, S., Intikhab, S., Profitt, L., Li, Y., Natu, V., Gawas, R. & Snyder, J.
 Nanoporous multimetallic Ir alloys as efficient and stable electrocatalysts for acidic

- oxygen evolution reactions. J. Catal. 393, 303–312 (2021).
- 31. Seitz, L. C., Dickens, C. F., Nishio, K., Hikita, Y., Montoya, J., Doyle, A., Kirk, C., Vojvodic, A., Hwang, H. Y., Norskov, J. K. & Jaramillo, T. F. A highly active and stable IrO x /SrIrO 3 catalyst for the oxygen evolution reaction. *Science* (80-.). **353**, 1011–1014 (2016).
- 32. Creczynski, G., Hultman, L. C 1s peak of adventitious carbon aligns to the vacuum level: dire consequences for material's bonding assignment by photoelectron spectroscopy.

 *ChemPhysChem 18, 1507–1512 (2017).
- 33. Erlebacher, J. An Atomistic Description of Dealloying. *J. Electrochem. Soc.* **151,** C614–C626 (2004).
- Erlebacher, J., Sieradzki, K. Pattern formation during dealloying. Scr. Mater. 49, 991–996
 (2003).
- 35. Giesen, M., Beltramo, G., Dieluweit, S., Muller, J., Ibach, H., Schmickler, W. The thermodynamics of electrochemical annealing. *Surf. Sci.* **595**, 127–137 (2005).
- 36. Sharma, A., Bhattarai, J., Alla, A., Demchenko, A., Stine, K. Electrochemical annealing of nanoporous gold by application of cyclic potential sweeps. *Nanotechnology* **26**, 085602 (2015).
- 37. Sun, C. Q., Wang, Y., Tay, B. K., Li, S., Huang, H. & Zhang, Y. B. Correlation between the melting point of a nanosolid and the cohesive energy of a surface atom. *J. Phys. Chem. B* **106**, 10701–10705 (2002).
- 38. Li, X., Chen, Q., McCue, I., Snyder, J., Crozier, P., Erlebacher, J. & Sieradzki, K. Dealloying of noble-metal alloy nanoparticles. *Nano Lett.* **14**, (2014).
- 39. Erlebacher, J., Aziz, M. J., Karma, A., Dimitrov, N. & Sieradzki, K. Evolution of

- nanoporosity in dealloying. Nature 410, 450–453 (2001).
- 40. Pourbaix, M. Atlas of Electrochemical Equilibria in Aqueous Solutions. (NACE International, 1974).
- 41. Erlebacher, J. An Atomistic Description of Dealloying. *J. Electrochem. Soc.* **151,** C614–C626 (2004).

Figures



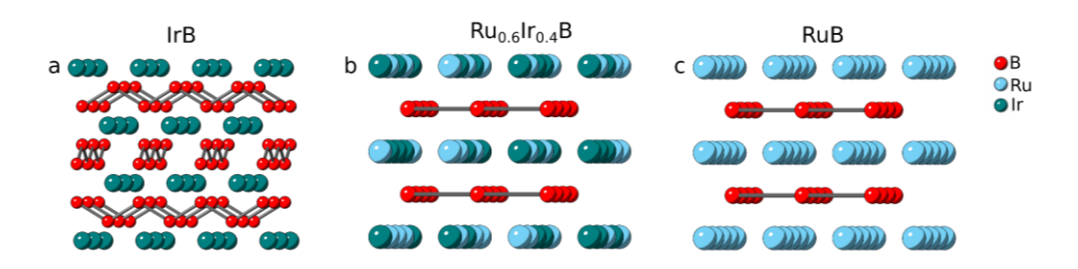


Figure 1: (top) Experimental XRD patterns of Ru_{0.6}Ir_{0.4}B (black), IrB (red) and RuB (pink). Theoretical XRD patterns for IrB (blue) and RuB (green). (bottom) Crystal structures for (a) IrB, (b) Ru_{0.6}Ir_{0.4}B, and (c) RuB.

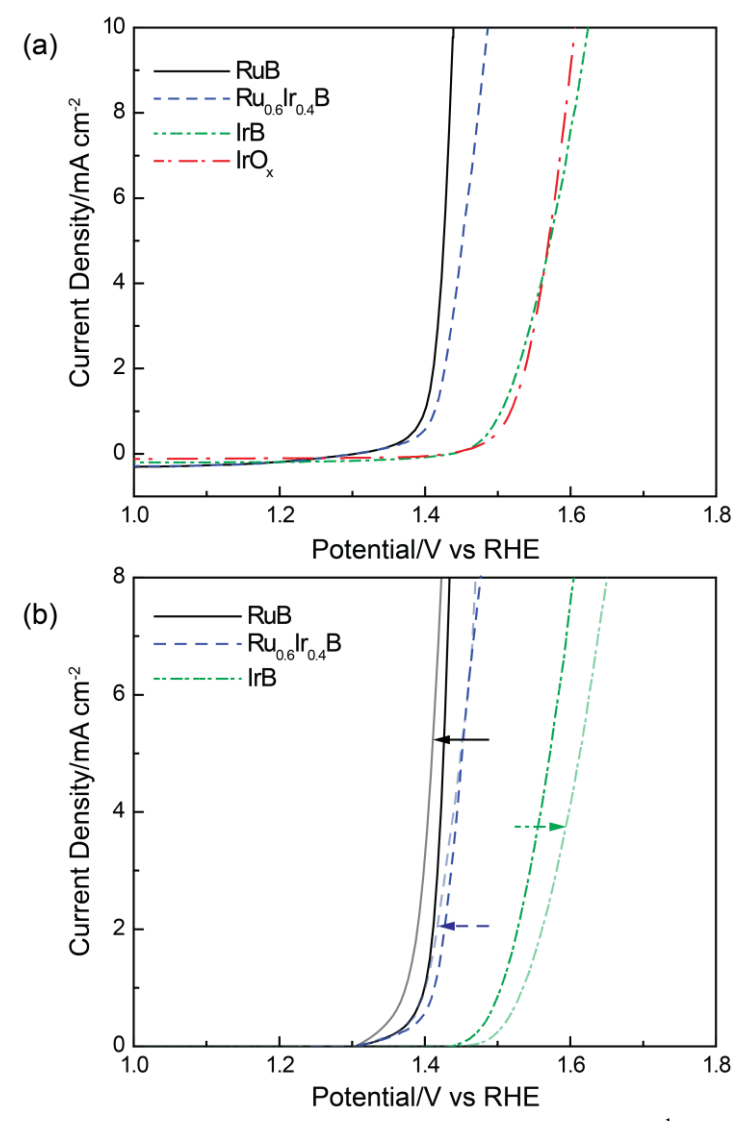


Figure 2: OER polarization curves at 20 mV s⁻¹ in Ar purged 0.1 M HClO₄ for (a) initial, as-synthesized borides and (b) after 1000 potential cycles (dealloying) from 0.5 V to 1.5 V vs. RHE. RuB (black), RuIrB (blue dashed), IrB (green dashed), and IrO_x (control; red dashed). Darker lines in (b) correspond to the as-synthesized material (data in (a)) and lighter lines are the OER polarization curves following the load cycling protocol. Arrows indicate change following load cycling.

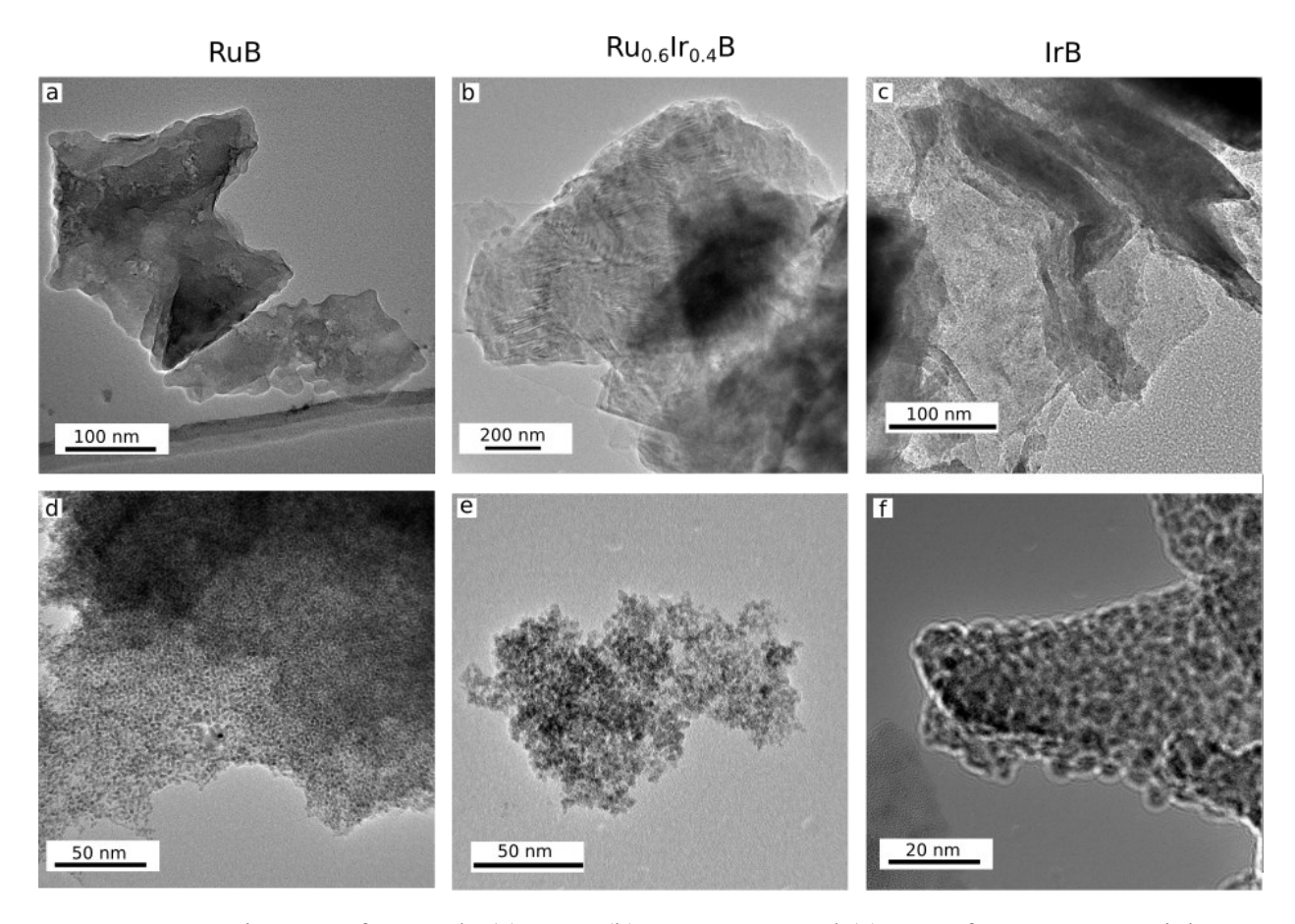


Figure 3: TEM images of as-made (a) RuB, (b) $Ru_{0.6}Ir_{0.4}B$, and (c) IrB; after 1000 potential cycles (d) RuB, (e) $Ru_{0.6}Ir_{0.4}B$, and (f) IrB.

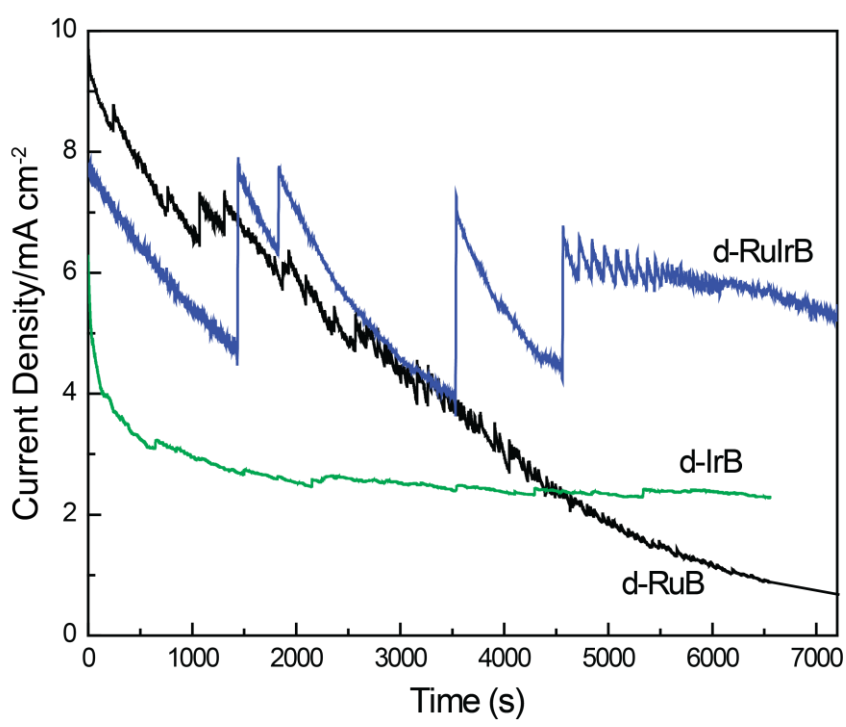


Figure 4: Constant potential electrolysis (chronoamperometric OER) transient current density for d-RuB (black), d-RuIrB (blue), d-IrB (green). Prior to electrolysis, all electrodes are put through 1000 load cycles to drive dealloying.